Electronic Supplementary Information

First-principles insight into CO hindered agglomeration of Rh and Pt single atoms on m-ZrO_2

Minttu M. Kauppinen, Marko M. Melander, and Karoliina Honkala*

Nanoscience Center, P.O. Box 35 (YN) FI-40014, Department of Chemistry, University of Jyväskylä, Finland

E-mail: karoliina.honkala@jyu.fi

1 Single atom formation energy

The formation energy $E_{\mathrm{sa}}^{\mathrm{f}}$ of a single atom species with respect to the bulk metal is calculated as

$$E_{\mathrm{sa}}^{\mathrm{f}} = E_{\mathrm{sa/ox}} - E_{\mathrm{ox}} - E_{\mathrm{bulk}} \tag{1.0.1}$$

where $E_{\mathrm{sa/ox}}$ is the energy of the supported single atom, E_{ox} is the energy of the oxide slab, and E_{bulk} is the energy of a metal atom in the bulk metal.[1] The calculated formation energies of single atoms on different zirconia sites (see Figures S2 and S3) are tabulated below (Table S1).

Table S1: Formation energies E^f_{sa} of Rh and Pt single atoms on ideal and defected zirconia sites.

		E^f_{sa} / eV (bader charge on metal atom)		
Metal	ZrO_2 facet	ad-atom	O_{vac}	Zr_{vac}
Rh	$(\bar{1}11)$	3.44(+0.15)	0.49(−0.84)	−3.89(+1.42)
Rh	$(\bar{2}12)$	2.61(+0.08)	0.92(−0.71)	-
Pt	$(\bar{1}11)$	2.93(−0.02)	−1.60(−1.10)	−3.33(+1.46)
Pt	$(\bar{2}12)$	1.29(−0.10)	−1.02(−0.95)	-

2 Oxygen and zirconium vacancy formation energy

The thermodynamic cost of removing an oxygen atom from the zirconia slabs, i.e. the reduction energy ΔE_{red}, can be evaluated as

$$\Delta E_{\mathrm{red}} = E_{\mathrm{vac}} + (E_{\mathrm{H_2O}} - E_{\mathrm{H_2}}) - E_{\mathrm{slab}} \tag{2.0.1}$$

where E_{vac} is the total energy of the slab with one lattice oxygen removed, $E_{\mathrm{H_2O}}$ and $E_{\mathrm{H_2}}$ are the gas phase energies of water and hydrogen molecules, respectively, and E_{slab} is the energy of the stoichiometric zirconia slab. Equation 2.0.1 describes the reduction of the zirconia surface with H_2 as the reducing species. The choice of gas-phase reference avoids the problem of using molecular oxygen as a reference.[2,3]

The cost of removing a zirconium atom is the defect formation energy, $\Delta E^f_{\mathrm{def}}$ which can be defined in a similar manner to the method in ref 4:

$$\Delta E^f_{\mathrm{def}} = E^{\mathrm{def}}_{\mathrm{slab}} - E_{\mathrm{slab}} + E^{\mathrm{Zr}}_{\mathrm{bulk}} \tag{2.0.2}$$

where $E^{\mathrm{def}}_{\mathrm{slab}}$ and E_{slab} are the total electronic energies of the zirconium defected slab and the defect free slab, respectively, and $E^{\mathrm{Zr}}_{\mathrm{bulk}}$ is the energy of a zirconium atom in the bulk metal.

3 Agglomeration energy

The agglomeration energy ΔE_{agg} of N single atoms (or single atom with n adsorbed CO) into a cluster consisting of N metal atoms (with $n \times N$ adsorbed CO molecules) per atom (ΔE_{agg}) and in total ($\Delta E_{\mathrm{agg}}^{total}$) are calculated as

$$\Delta E_{\mathrm{agg}} = \frac{1}{N}(E_{\mathrm{M}_N/\mathrm{ox}} - E_{\mathrm{ox}}) - (E_{\mathrm{sa/ox}} - E_{\mathrm{ox}}) \tag{3.0.1}$$

and

$$\Delta E_{\mathrm{agg}}^{total} = (E_{\mathrm{M}_N/\mathrm{ox}} - E_{\mathrm{ox}}) - N(E_{\mathrm{sa/ox}} - E_{\mathrm{ox}}) \tag{3.0.2}$$

where $E_{\mathrm{sa/ox}}$ is the energy of the supported single atom (with n adsorbed CO molecules), N is the number of single atoms/atoms in the reference cluster, E_{ox} is the energy of the oxide slab, $E_{\mathrm{M}_N/\mathrm{ox}}$ is the energy of the reference metal cluster (with $n \times N$ adsorbed CO molecules), and E_{CO} is the energy of CO in gas-phase.

In the case of the Zr substituted and oxygen vacancy containing surfaces the agglomeration of N single atoms into a cluster sitting on one of the vacancy sites (at the vacancy concentration considered here) leaves $N - 1$ unfilled vacancies on the surface. However, one can also consider the single atom sitting in a zirconium/oxygen vacancy as a kind of nucleation site with the rest of the metal atoms coming from SA species located on the ideal terrace. This way the resulting cluster contains only one metal atom in a oxygen or zirconium vacancy, with no unfilled vacancies left behind. The change in energy was calculated for both cases of agglomeration on defected surfaces resulting in two values ΔE_{agg} and $\Delta E_{\mathrm{agg}}^{nuc}$, respectively. The $\Delta E_{\mathrm{agg}}^{nuc}$ values are more analogous to the ΔE_{agg} values calculated for the pristine zirconia supported structures, and shall be used to describe the agglomeration energy in all discussions unless otherwise stated. Note that for the zirconium vacancy containing zirconia the clusters are considered to be the N metal atoms on top of the metal atom that substitutes for the missing zirconium atom. The calculated agglomeration energies

per atom are tabulated below (Tables S2, S3, S4).

Table S2: Agglomeration energies ΔE_{agg} of N Rh and Pt single atoms into N atom clusters on zirconia ($\bar{1}11$) in eV per atom.

	ΔE_{agg}	
N	Rh	Pt
2	−0.49	−0.51
3	−0.78	−0.77
4	−1.38	−1.29
13	−1.78	−1.37
19	−1.93	−1.45
43	−2.13	−1.73

Table S3: Agglomeration energies ΔE_{agg} and $\Delta E_{\mathrm{agg}}^{nuc}$ of N Rh and Pt single atoms into N atom clusters on zirconia ($\bar{1}11$) in the presence of an oxygen vacancy in eV per atom.

	Rh		Pt	
N	ΔE_{agg}	$\Delta E_{\mathrm{agg}}^{nuc}$	ΔE_{agg}	$\Delta E_{\mathrm{agg}}^{nuc}$
2	0.66	−0.75	1.58	−0.56
3	0.54	−1.34	2.09	−0.76
4	0.83	−1.28	2.44	−0.78

Table S4: Agglomeration energies ΔE_{agg} and $\Delta E_{\mathrm{agg}}^{nuc}$ of N Rh and Pt single atoms into N atom clusters on metal substituted zirconia ($\bar{1}11$) in eV per atom.

	Rh		Pt	
N	ΔE_{agg}	$\Delta E_{\mathrm{agg}}^{nuc}$	ΔE_{agg}	$\Delta E_{\mathrm{agg}}^{nuc}$
2	3.94	−1.29	3.41	−0.91
3	4.26	−1.53	3.61	−1.21
4	5.56	−1.64	3.84	−1.22

4 Adhesion energy

The adhesion energy ΔE_{adh} of the clusters to the oxide support is defined as

$$\Delta E_{\mathrm{adh}} = E_{\mathrm{M}_N/\mathrm{ox}} - E_{\mathrm{ox}} - E_{\mathrm{M}_N} \tag{4.0.1}$$

where E_{M_N} is the energy of the metal cluster in gas phase constrained to the supported cluster geometry. The multiplicities of the gas-phase clusters are reported in Table S5. The calculated adhesion energies are presented in tables S6, S7, and S8.

Table S5: Multiplicities of the gas-phase Rh and Pt clusters constrained to the supported cluster geometry.

	Multiplicity	
N	Rh	Pt
1	doublet	triplet
2	quintet	triplet
3	quartet	singlet
4	singlet	triplet

Table S6: Adhesion energies ΔE_{adh} of Rh and Pt species on $ZrO_2(\bar{1}11)$ with N atoms in eV.

	ΔE_{adh}	
N	Rh	Pt
1	−2.44	−2.46
2	−2.36	−2.56
3	−2.35	−3.92
4	−3.72	−4.70

Table S7: Adhesion energies ΔE_{adh} of Rh and Pt species on $ZrO_2(\bar{1}11)$ with oxygen vacancy with N atoms in eV.

	ΔE_{adh}	
N	Rh	Pt
1	−5.39	−6.99
2	−6.10	−7.57
3	−7.34	−7.98
4	−6.96	−8.22

5 Atomistic Thermodynamics

Atomistic thermodynamics[5–7] calculations were employed in order to evaluate the stability of supported SA and clusters at elevated temperatures and under a CO atmosphere. The surface free energy change, $\Delta\gamma_S$, to the M-ZrO_2 catalyst upon adsorption of CO is defined

Table S8: Adhesion energies ΔE_{adh} of Rh and Pt species on metal substituted $ZrO_2(\bar{1}11)$ with N atoms in eV.

	ΔE_{adh}	
N	Rh	Pt
1	−3.77	−3.28
2	−3.95	−3.82
3	−5.96	−4.80
4	−5.67	−5.29

as

$$\Delta\gamma_{\text{S}}(T,p) = \frac{1}{A}\left(G_{\text{CO-M/ox}}(T,p) - G_{\text{M/ox}}(T,p) - n\mu_{\text{CO}}(T,p)\right) \tag{5.0.1}$$

where A is the surface area of the oxide unit cell, $G_{\text{CO-M/ox}}$ is the free energy of the SA or cluster containing oxide surface modified by adsorbed CO, $G_{\text{M-ox}}$ is the free energy of the oxide supported SA or cluster, μ_{CO} is the chemical potential of the gas-phase CO molecule, and n is the number of adsorbed molecules present on the surface. The expression in the brackets is the free energy change of CO adsorption, $\Delta G_{\text{CO}}(T,p)$. The free energy of the M-ZrO_2 system is approximated to be equal to its electronic energy, $E_{\text{M/ox}}$. For the M-ZrO_2 species with adsorbed CO the free energy at temperature T is approximated as the electronic energy $E_{\text{CO-M/ox}}$ corrected by the zero-point energy $E^{\text{ZPE}}_{\text{CO-M/ox}}$ and the vibrational entropy contribution from the adsorbed CO molecules, S_{vib}, calculated in the harmonic approximation as implemented in ASE.[8,9]

$$G_{\text{CO-M/ox}} \approx E_{\text{CO-M/ox}} + E^{\text{ZPE}}_{\text{CO-M/ox}} - S_{vib} * T \tag{5.0.2}$$

The chemical potential of CO is

$$\mu_{\text{CO}}(T,p) = E_{\text{CO}} + E^{\text{ZPE}}_{\text{CO}} + \underbrace{\mu^{\circ}_{\text{CO}}(T,p^{\circ}) + k_b T \ln\frac{p}{p^{\circ}}}_{\Delta\mu_{\text{CO}}(T,p)} \tag{5.0.3}$$

where E_{CO} is the electronic energy of the CO molecule in gas-phase, $E^{\text{ZPE}}_{\text{CO}}$ is the zero-point energy of the CO molecule, $\mu^{\circ}_{\text{CO}}(T)$ is the standard chemical potential of CO taken

from the NIST-JANAF thermochemical tables,[10] k_b is the Boltzmann constant, T is the absolute temperature, p is the CO partial pressure and p° is the standard pressure. A negative (positive) value of $\Delta\gamma_S$ indicates stabilization (destabilization) of the M-ZrO_2 upon adsorption of n adsorbate species.

6 CO adsorption energies, stretching frequencies, & support ligand effect on CO binding

CO adsorption energies and vibrational frequencies of CO stretching modes of CO bonded to zirconia supported SA and small clusters are listed in Table S9. The adsorption energies are reported as average and differential energies.

The quantity $\Delta\Delta E_{\text{ads}}$ describes the ligand effect that the support has on the strength of CO adsorption and is defined as the difference between the adsorption energy of CO on the supported cluster, ΔE_{ads}, and the adsorption energy of CO on an unsupported cluster, $\Delta E_{\text{ads}}^{unsupp}$, with the atoms constrained to the supported cluster geometry.

$$\Delta\Delta E_{\text{ads}} = \Delta E_{\text{ads}} - \Delta E_{\text{ads}}^{unsupp} \tag{6.0.1}$$

A negative (positive) value of $\Delta\Delta E_{\text{ads}}$ indicates a stabilising (de-stabilising) ligand effect on CO adsorption by the support. The calculated values are presented in Tables S12, S13, and S14.

Table S9: Adsorption energies of CO in eV and vibrational frequencies ν(CO) of CO stretching in cm^{-1} for CO adsorbed on SA and small clusters on $ZrO_2(\bar{1}11)$.

		M/$ZrO_2(\bar{1}11)$		
species	n CO	E_{ads}^{diff}	E_{ads}^{av}	ν(CO)
Rh_1	1	−2.99	−2.99	1956
	2	−1.54	−2.27	1976, 1936
	3	−0.87	−1.80	2008, 1964, 1948
Pt_1	1	−3.47	−3.47	2037
	2	−0.62	−2.04	2023, 1993
	3	−0.86	−1.65	2074, 2018, 2010
Rh_2	1	−3.31	−3.31	1951
	2	−2.92	−3.12	1997, 1959
	3	−1.44	−2.56	2002, 1978, 1777
	4	−1.44	−2.28	2040, 1984, 1970, 1942
	5	−1.26	−2.08	2051, 2014, 2002, 1967, 1896
	6	−0.41	−1.80	2082, 2035, 2021, 1990, 1954, 1919
Pt_2	1	−3.89	−3.89	1844.8
	2	−1.75	−2.82	2061, 2022
Rh_3	1	−3.39	−3.39	1975
	2	−2.79	−3.09	2002, 1968
	3	−2.32	−2.84	2014, 1976, 1957
	4	−1.38	−2.47	2011, 1981, 1966, 1810
	5	−0.98	−2.17	2027, 1994, 1985, 1974, 1907
	6	−1.51	−2.06	2053, 2002, 1987, 1959, 1869, 1838
Pt_3	1	−3.30	−3.30	2048
	2	−2.87	−3.09	1898, 1855
	3	−1.53	−2.57	2017, 1934, 1843
Rh_4	1	−2.28	−2.28	1958
	2	−2.02	−2.15	1966, 1953
	3	−2.96	−2.42	1982, 1953, 1851
	4	−2.55	−2.45	1992, 1965, 1842, 1827
	5	−1.29	−2.22	2028, 1992, 1961, 1902, 1852
	6	−1.11	−2.03	2043, 1999, 1963, 1944, 1928, 1836
Pt_4	1	−2.14	−2.14	2006
	2	−2.37	−2.25	2050, 2030
	3	−2.84	−2.45	2034, 1888, 1853
	4	−0.40	−1.94	2054, 2040, 2027, 1985

Table S10: Adsorption energies of CO in eV and vibrational frequencies ν(CO) of CO stretching in cm^{-1} for CO adsorbed on SA and small clusters on $ZrO_2(\bar{1}11)$ with an oxygen vacancy.

		$M/ZrO_2(\bar{1}11)_{Ovac}$		
species	n CO	E_{ads}^{diff}	E_{ads}^{av}	ν(CO)
Rh_1	1	−2.38	−2.38	1893
	2	−1.48	−1.92	1963, 1705
	3	−1.25	−1.70	1969, 1907, 1857
	4	−0.20	−1.33	2041, 1957, 1882, 1803
Pt_1	1	−0.78	−0.78	2021
	2	−1.17	−0.97	2005, 1985
	3	−0.91	−0.95	2040, 2005, 1993
Rh_2	1	−3.89	−3.89	1800
	2	−0.47	−2.18	1987, 1949
	3	−1.39	−1.92	1989, 1957, 1949
	4	−0.98	−1.68	1989, 1963, 1953, 1860
Pt_2	1	−2.09	−2.09	2001
	2	−0.83	−1.46	2018, 1897
	3	−0.86	−1.26	2056, 2021, 2001
	4	−0.78	−1.14	2076, 2013, 1989, 1974
Rh_3	1	−2.92	−2.92	1695
	2	−1.74	−2.33	1961, 1813
	3	−1.36	−2.01	1945, 1922, 1884
Pt_3	1	−2.44	−2.44	1981
	2	−1.05	−1.75	2007, 1877
	3	−1.93	−1.81	2018, 1995, 1900
Rh_4	1	−2.57	−2.57	1943
	2	−2.43	−1.67	1950, 1822
	3	−0.93	−1.98	1987, 1947, 1938
	4	−2.47	−2.80	2018, 1978, 1960, 1946
Pt_4	1	−1.89	−1.89	2009
	2	−2.49	−2.19	2038, 2000
	3	−2.40	−2.26	2062, 2041, 2020
	4	−0.64	−1.85	2057, 2043, 2025, 2001

Table S11: Adsorption energies of CO in eV and vibrational frequencies ν(CO) of CO stretching in cm^{-1} for CO adsorbed on SA and small clusters on metal substituted $ZrO_2(\bar{1}11)$

		$M/ZrO_2(\bar{1}11)_{subs}$		
species	n CO	E_{ads}^{diff}	E_{ads}^{av}	ν(CO)
Rh_{sub}	1	−1.66	−1.66	2061
Pt_{sub}	1	−1.53	−1.53	2130
Rh_1	1	−2.69	−2.69	1991
	2	−2.95	−2.82	2068, 2007
Pt_1	1	−3.60	−3.60	2044
	2	−1.14	−2.37	2086, 2044
Rh_2	1	−3.08	−3.08	1964
	2	−2.55	−2.82	1995, 1952
	3	−0.99	−2.21	2054, 2014, 1944
	4	−2.60	−2.31	2063, 2043, 2009, 1996
Pt_2	1	−3.11	−3.11	2043
	2	−2.62	−2.87	2047, 2022
	3	−1.10	−2.28	2094, 2057, 2005
	3	−0.56	−1.85	2096, 2060, 1996, 1954
Rh_3	1	−3.13	−3.13	1968
	2	−2.31	−2.72	1985, 1949
	3	−2.44	−2.63	1997, 1973, 1958
Pt_3	1	−2.50	−2.50	2048
	2	−2.36	−2.43	2045, 2021
	3	−0.72	−1.86	2052, 2022, 2013
Rh_4	1	−3.70	−3.70	1956
	2	−2.51	−3.11	2005, 1963
	3	−2.01	−2.74	2007, 1970, 1948
	4	−1.93	−2.54	2011, 1979, 1968, 1723
Pt_4	1	−2.34	−2.34	2033
	2	−2.74	−2.54	2049, 2025
	3	−1.71	−2.26	2033, 2013, 1859
	4	−1.82	−2.15	2056, 2029, 2007, 1876

Table S12: $\Delta\Delta E_{ads}$ for a single adsorbed CO on Rh and Pt clusters with N atoms in eV, originally deposited on the ideal $ZrO_2(\bar{1}11)$

	$\Delta\Delta E_{ads}$	
N	Rh	Pt
1	+0.18	+0.05
2	−1.30	−0.86
3	−1.55	−2.03
4	−0.16	−0.63

Table S13: $\Delta\Delta E_{\text{ads}}$ for a single adsorbed CO on Rh and Pt clusters with N atoms in eV, originally deposited on $ZrO_2(\bar{1}11)$ with an oxygen vacancy.

	$\Delta\Delta E_{\text{ads}}$	
N	Rh	Pt
1	+0.75	+2.09
2	−1.49	+0.21
3	−0.65	+0.05
4	−0.43	+0.19

Table S14: $\Delta\Delta E_{\text{ads}}$ for a single adsorbed CO on Rh and Pt clusters with N atoms in eV, originally deposited on $ZrO_2(\bar{1}11)$ with a metal atom substituting one Zr atom.

	$\Delta\Delta E_{\text{ads}}$	
N	Rh	Pt
1	+0.45	−0.09
2	−1.34	−1.36
3	−1.18	−0.92
4	−2.93	+0.14

7 Estimating the kinetic stability of single atoms

To assess the kinetic stability of SAs, a scheme based on non-equilibrium thermodynamics is developed below. In this treatment, the initially deposited SAs diffuse on the surface and upon collision may grow into larger clusters. As we are dealing with small clusters, the thermodynamic potentials are, in general, non-extensive and Hill's approach to nanothermodynamics[11–13] is adopted.

7.1 Rate of entropy production due to diffusion in macroscopic systems

In non-equilibrium thermodynamics, irreversible changes are controlled by entropy production which drives the system towards an equilibrium state. For diffusion systems without temperature or pressure gradients or chemical reactions, the rate of entropy production is[14]

$$\frac{dS}{dt} = -\frac{1}{T}\sum_{k=1}^{n} J_k(t) \cdot [T\nabla\mu_k(T)/T] \geq 0 \tag{7.1.1}$$

where the chemical potential difference is the thermodynamic driving force and J_k is the (time-dependent) flux. To simplify the notation, the time-dependence of the chemical potentials and fluxes is not explicitly denoted below and it is implicit that these quantities depend on time. For a diffusion problem the flux is written as[14,15]

$$J_k = -L(\nabla\mu_k)_{T,P} \tag{7.1.2}$$

where L is a phenomenological transport coefficient. Inserting the flux in the definition of the entropy production gives (here for a 1D, one component system)

$$\frac{dS}{dt} = \frac{1}{T}a(\nabla\mu_k)_{T,P} \cdot [T\nabla\mu_k/T] = \frac{L}{T}(\nabla\mu_k)^2_{P,T} \geq 0 \tag{7.1.3}$$

which shows that if a chemical potential gradient exists in a system, the rate of entropy

production is positive. Equilibrium (or steady-state) is reached when the gradient disappears and the transport coefficient defines the rate of this transformation.

7.2 Flux due to diffusion

A material flux in a system exists until the chemical potential is constant throughout the system. As shown, the flux (both direction and magnitude) depends on the chemical potential gradient:

$$J_k = -L(\nabla\mu_k)_{T,P} = -L\left(\frac{\partial\mu_k}{\partial c_k}\right)_{P,T}\nabla c_k = -D\nabla c_k \tag{7.2.1}$$

where c_k is the (surface) concentration and $D = L(\partial\mu_k/\partial c_k)$ is identified as a diffusion "coefficient"; it is to be noted that the diffusion "coefficient" depends not only on the phenomenological transport coefficient L, but also on the chemical potential gradient in the system. Hence, diffusion is faster in a system far away from equilibrium (larger $\nabla\mu_k$). As shown in Ref. 16, the surface diffusion coefficient can be written as

$$D = r_k(c_k)\frac{\partial\mu_k}{\partial c_k} \tag{7.2.2}$$

where r_k is the diffusion jump rate which also depends on the concentration. r_k is considered as an activated transition and has the form of a thermal rate equation

$$r_k = \lambda^2\frac{k_BT}{h}\exp[-\Delta G^{\ddagger}(c_k)/k_BT] \tag{7.2.3}$$

where $\Delta G_k(c_k)$ is the concentration dependent activation energy and λ^2 is the mean-square jump distance. Finally, the diffusion flux is given as

$$J_k = r_k\left(\frac{\partial\mu_k}{\partial c_k}\right)_{T,P}\nabla c_k \tag{7.2.4}$$

7.3 Thermodynamics of small systems: Nanothermodynamics

The treatment of nanothermodynamics relies on the work of Hill[11,12,17]. The main idea behind nanothermodynamics is that small enough systems are no longer extensive in a thermodynamic sense. To account for the non-extensivity observed in nanoscopic systems, Hill introduced the subdivision potential **E**. To understand the role of **E**, one performs a thought experiment. A macroscopic system with N_t atoms/particles is divided into **N** independent subsystems each consisting of N atoms: $N_t = N\mathbf{N}$. The change in internal energy is

$$dU_t = TdS_t - pdV_t + \mu dN_t \tag{7.3.1}$$

If the system is extensive (guaranteed if all subsystems are macroscopic), the internal energy is a first order homogeneous function of (S_t, N_t, V_t) which satisfies

$$U_t = TS_t - pV_t + \mu N_t \tag{7.3.2}$$

Now consider the internal energy as a function of **N**. If it is observed that $U_t(S_t, N_t, V_t, \mathbf{N}_1) \neq U_t(S_t, N_t, V_t, \mathbf{N}_2)$, the systems is no longer extensive; the internal energy of the system depends on the number and size of the independent subsystems. In this case, the total internal energy change must be accompanied by a new quantity **E** - the sub-division potential. Hence, the internal energy change is written as

$$dU_t = TdS_t - pdV_t + \mu dN_t + \mathbf{E}d\mathbf{N} = TdS_t - pdV_t + (\mu N + \mathbf{E})d\mathbf{N} \tag{7.3.3}$$

in terms of the conjugate quantities (T, S_t), (p, V_t), (μ, N_t), and (**E,** **N**). As the composite system is homogeneous in its extensive variables, one has

$$U_t = TS_t - pV_t + \mu N_t + \mathbf{EN} \tag{7.3.4}$$

and by definition:

$$S_t = \mathbf{N}S, \quad U_t = U\mathbf{N}, \quad V_t = \mathbf{N}V, \quad N_t = \mathbf{N}N \tag{7.3.5}$$

Dividing both sides of this equation by $\mathbf{N}$, one obtains the Gibbs equation for the internal energy and Gibbs energy of a single subsystem

$$U = TS - pV + \mu N + \mathbf{E} \quad \text{and} \quad G = \mu N + \mathbf{E} \tag{7.3.6}$$

From the last equation, the generalized chemical potential $\hat{\mu}$ is defined as

$$\hat{\mu} \equiv \frac{G}{N} = \mu + \frac{\mathbf{E}}{N} \tag{7.3.7}$$

which can also be identified as the last term of Eq. (7.3.3). By definition $\lim_{N\to\infty} \hat{\mu} = \mu$, because the subdivision potential vanishes for macroscopic objects. From these definitions it also follows that

$$G_t(\mathbf{N}) = G(\mathbf{N})\mathbf{N} = \hat{\mu}(\mathbf{N})N\mathbf{N} = \hat{\mu}(\mathbf{N})N_t \tag{7.3.8}$$

7.4 Entropy production in nanoscopic systems: A simple treatment of diffusion in nanosystems

The development in the previous section can also be transferred to non-equilibrium situations. As discussed in 7.1 and 7.2, the key thermodynamic driving force to transport and diffusion is the entropy production. For a nanosystem one needs to consider the *total entropy production* dS_t/dt.[18]

Consider two nanosystems A and B (in our case these are ensembles of different sized clusters) corresponding to the treatment in Ref. 18. The composite $A+B$ is isolated from the surroundings and initially out of equilibrium with $\mathbf{N}_A^0$ and $\mathbf{N}_B^0$. The entropy change during equilibration is $\Delta S_t = S_t - S_t^{eq} = \Delta S_{A,t} + \Delta S_{B,t}$ and the equilibration rate is $\dfrac{d\Delta S_t}{dt}$. Also the

subdivisions are functions of time, hence $\mathbf{N}_i^0 \neq \mathbf{N}_i^{eq}$. The resulting entropy production rate and fluxes were analyzed in detail in Ref. 18 and the complicated forms are not reproduced here; the crucial point from general *non-equilibrium nanothermodynamics development* is that *entropy production rate retains the same form as in the macroscopic non-equilibrium thermodynamics*. In other words, approach towards equilibrium is driven by entropy production which depends on fluxes and thermodynamic driving forces. The essential new term is related to the time-dependent destruction/production of new subdivisions.

In order to understand the irreversible $A \rightarrow B$ transformation, a simple non-equilibrium (nano)thermodynamic model is constructed. As discussed, the relevant quantity is the entropy production and its rate in the transition from an initial to final state, as depicted in Fig. S1. In the present case, the system is initially characterized by fully dispersed atoms *i.e.* SAs supported on surface and $N_A = 1$. This corresponds to $\mathbf{N}_A = \gamma$ as the number of subdivisions. In the final state, the initially dispersed atoms have formed a larger cluster $N_B = \gamma$, and $\mathbf{N}_B = N_t/\gamma$. In both systems the total number of atoms is N_t.

Figure S1: Particle growth from single atoms on a surface

In this case, γ is also the order parameter quantifying the change from $A \rightarrow B$. For instance, γ can be taken as the surface coverage of the single atoms. Evolution from A to B takes place *via* surface diffusion. For such a system, the entropy production rate is[19]

$$\frac{dS_t}{dt} = -\frac{1}{T}\int J(\gamma)\frac{\partial \hat{\mu}(\gamma,t)}{\partial \gamma(t)}\mathrm{d}\gamma(t) \tag{7.4.1}$$

in terms of the generalized chemical potential introduced in Eq. (7.3.7). The flux $J(\gamma)$ denotes the flux along the γ pathway *i.e.* it is the macroscopic diffusion current characterising the $A \rightarrow B$ transition. One can describe the flux as a diffusion over the free-energy barrier using Eq. (7.2.4) but now in terms of the generalized chemical potential, $D(\gamma)$. The macroscopic diffusion rate is also characterised by the phenomenological (Onsager-like) co-

efficient L which is related to the flux through Eq. (7.1.2). Note that Eq.(7.2.4) defines the rate for an atom to jump from one site to another while $D(\gamma), L(\gamma)$ and $J(\gamma)$ characterise the transition rate of the entire system from state A to state B. The surface concentration of the single atoms acts as the reaction coordinate. Introducing these definitions in the above equation leads to entropy production rate in the form

$$\begin{aligned} \frac{dS_t}{dt} &= \frac{1}{T}\int \frac{L(\gamma)}{T}\frac{\partial\hat{\mu}}{\partial\gamma}\frac{\partial\hat{\mu}(\gamma)}{\partial\gamma(t)}\mathrm{d}\gamma(t) \\ &= \frac{1}{T}\int D(\gamma)\frac{\partial\hat{\mu}}{\partial\gamma}\mathrm{d}\gamma(t) \end{aligned} \tag{7.4.2}$$

To advance, the approach in Ref. 19 is followed. The generalized chemical potential along the reaction path is used for defining a generalised fugacity: $z(\gamma) = \exp[\hat{\mu}(\gamma)/k_BT]$. With this definition the entropy production rate becomes

$$\begin{aligned} \frac{dS_t}{dt} &= \frac{1}{T}\int \frac{k_BL(\gamma)}{z(\gamma)}\frac{\partial z(\gamma)}{\partial\gamma}\frac{\partial\hat{\mu}(\gamma,t)}{\partial\gamma(t)}\mathrm{d}\gamma(t) \\ &= -\frac{1}{T}\int J(\gamma)\frac{\partial\hat{\mu}(\gamma,t)}{\partial\gamma(t)}\mathrm{d}\gamma(t) \end{aligned} \tag{7.4.3}$$

and the flux is identified as $J = -k_BL\frac{1\partial z}{z\partial\gamma} = -D\frac{\partial z}{\partial\gamma}$. To evaluate the flux magnitude at time instant t, the flux is integrated from the initial A to final B state. The relevant flux measures the conversion rate from A to B and this is denoted as J_{AB}. The corresponding diffusion constant is D_{AB}. With these definitions one obtains the total flux as

$$\bar{J}_{AB} = \int_A^B J_{AB}(\gamma)\mathrm{d}\gamma = -\int_A^B D_{AB}\frac{\partial z}{\partial\gamma}\gamma \approx -D_{AB}(z_2 - z_1) \tag{7.4.4}$$

where it has been assumed that the diffusion constant between from A to B does not depend on γ i.e. the diffusion coefficient does not depend on the surface coverage in the present setting. Using the definition of the generalized fugacity leads to

$$\bar{J}_{AB} = -D_{AB}\left(\exp\left[\frac{\hat{\mu}_B}{k_B T}\right] - \exp\left[\frac{\hat{\mu}_A}{k_B T}\right]\right) \tag{7.4.5}$$

This equation can be understood as a diffusion from state A to state B. In the present case this means that the initial state SAs are transformed to larger clusters/particles. The bracketed term is the thermodynamical driving force (or affinity) from state A to B. If $\hat{\mu}_A = \hat{\mu}_B$ there is no thermodynamic driving force for the transition. Furthermore, if $D_{AB} = D_{BA}$ and $\hat{\mu}_A = \hat{\mu}_B$, $J_{AB} = J_{BA}$, there is no net flux between A and B. The diffusion coefficient D_{AB} characterizes the kinetic barrier needed to surmount when going from A to B along the reaction path γ and we distinguish between two situations: the free energy is either a 1) monotonously decreasing function of surface coverage or 2) the free energy is decreasing but non-monotonous. In 1) the free energy is always decreasing and there are no higher energy isomers between A and B. In this situation $D \propto \exp[-\Delta G^{\ddagger}/k_B T]$ i.e the diffusion constant is proportional to the transition state energy ($\Delta G^{\ddagger}$) for SA diffusion between sites. In 2), a higher energy isomer separates A and B in which case there is an extra thermodynamic penalty or barrier ($\Delta\hat{\mu}^{\ddagger}$) along the reaction pathway. In case 2), the $D \propto \exp[-(\Delta G^{\ddagger} + \Delta\hat{\mu}^{\ddagger})/k_B T]$. See the next section for more details.

7.5 Particle growth kinetics from non-equilibrium thermodynamics

The general non-equilibrium thermodynamic framework for assessing the stability of single atom catalysts was presented above. Here, it is described how the particle growth kinetics can be assessed from the general framework. As discussed, D_{AB} is an effective barrier separating the states A and B. In the present case, the evolution of the system takes place *via* surface diffusion of single atoms.

The rate equations for particles of different sizes are written as

$$\frac{dc_1}{dt} = -\sum_i k_{1\to i} c_1 + \sum_j k_{j\to 1} c_j \tag{7.5.1}$$

where k is the effective transition attachment (detachment) rate from (to) a particle. For each transition at steady state the detailed balance dictates that

$$k_{j\to 1} = k_{1\to j} \exp\left[-\frac{\Delta\hat{\mu}_{j\to 1}}{k_B T}\right] \tag{7.5.2}$$

This has the same form as Eq. (7.4.5). It is assumed that the surface diffusion is the rate-limiting process. Therefore, the relevant kinetic barrier along reaction coordinate γ is the rate surface diffusion rate. Diffusion coefficient D_{AB} is taken to equal the single atom diffusion coefficient. Assuming that the diffusion coefficient does not depend on the extent of the reaction (as done to arrive at Eq. (7.4.4)) is the same as assuming that the single atom diffusion coefficient is independent of the surface coverage or reaction extent.

With these definitions the total flux transforming 1 to j for a monotonous decrease in the generalised chemical potential (case 1) is given as

$$\bar{J}_{1\to j}^{\text{case 1}} \approx \frac{k_B T}{h} \exp[-\Delta G_{diff}^{\ddagger}/k_B T] \left(\exp\frac{\hat{\mu}_j}{k_B T} - \exp\frac{\hat{\mu}_1}{k_B T}\right) \tag{7.5.3}$$

If cluster size k is more unstable (higher generalised chemical potential) than the initial state i, an additional free energy barrier exists and for this non-monotonous decrease (case 2) the flux is

$$\bar{J}_{1\to j}^{\text{case 2}} \approx \frac{k_B T}{h} \exp[-(\Delta G_{diff}^{\ddagger} + \Delta\hat{\mu}_{i\to k}^{\ddagger})/k_B T] \left(\exp\frac{\hat{\mu}_j}{k_B T} - \exp\frac{\hat{\mu}_1}{k_B T}\right) \tag{7.5.4}$$

This shows that the rate of change from a single atom to a large particle depends on the diffusion kinetics of single atoms as well as the relative stability. A remarkably similar equation from a macroscopic perspective can also be developed[1] but the presented approach does not assume macroscopic thermodynamics and is therefore valid for all nanoparticle

sizes. The main results of the kinetic analysis are Eqs (7.5.3) and (7.5.4). The outcome from this development is that without a sizeable nucleation barrier, $\hat{\mu}_{i\to k}$, the SA will inevitably transform into larger clusters. The kinetics will depend on the diffusion barrier which sets the relevant time scale for the studies process.

We also note that within the taken approach explicit time-dependence can be investigated as follows. Writing the fluxes for all possible changes $i \to j$ gives a continuous, time-dependent flux along the reaction coordinate γ: $J(\gamma, t)$. With this, the time evolution of probability $P(\gamma, t)$ to observe different clusters can be solved from the continuity equation

$$\frac{\partial P(\gamma, t)}{\partial t} = -\frac{\partial}{\partial \gamma} J(\gamma, t) \tag{7.5.5}$$

This in turn can be analyzed using the Fokker-Planck equation as done in Ref. 20 but this is not within the scope of the present work.

8 Generalised chemical potentials

Generalised chemical potentials were calculated for subsystems with $N = 1, 2, 3, 4, 13, 19, 43$ for a system with $N_t = 10621$. The Gibbs free energy of a subsystem with N_x is taken to be the total electronic energy of the M_x/ZrO_2 catalyst model minus the energy of the oxide slab. The configuration entropy of a subsystem can be estimated using the formula

$$S^{\text{config}} = k_b(x \ln x - (x-1) \ln (x-1)) \tag{8.0.1}$$

where k_b is the Boltzmann constant and x is the reciprocal number of the fractional surface coverage (θ) of the subsystem.[21] If system A of N_t^A atoms consisting of $\mathbf{N}_A$ subsystems of single atoms (i.e. $N_A = 1$) has a coverage of θ, system B of N_t^B atoms consisting of $\mathbf{N}_B$ subsystems of N_B atoms will have a coverage of $\frac{\theta}{N_B}$ when $N_t^A = N_t^B$. For a SA surface coverage of 0.01 ML the configuration entropy per SA would be 4.83×10^{-4} eV / K, which

is a very small contribution to the generalised chemical potential even at high temperatures. For larger clusters S^{config} is even smaller, therefore the entropy is left out from the tabulated values, effectively meaning the values correspond to a temperature of 0 K. The values for $\hat{\mu}$ are presented in Table S15.

Table S15: Generalized chemical potentials, $\hat{\mu}$, of Rh and Pt SA and clusters with N atoms in eV at $0K$

	$\hat{\mu}$	
N	Rh	Pt
1	−4.07	−3.64
2	−4.38	−4.01
3	−4.66	−4.23
4	−5.25	−4.75
13	−5.65	−4.83
19	−5.79	−4.90
43	−6.0	−5.24
bulk	−7.31	−6.71

9 Catalyst model structure geometries

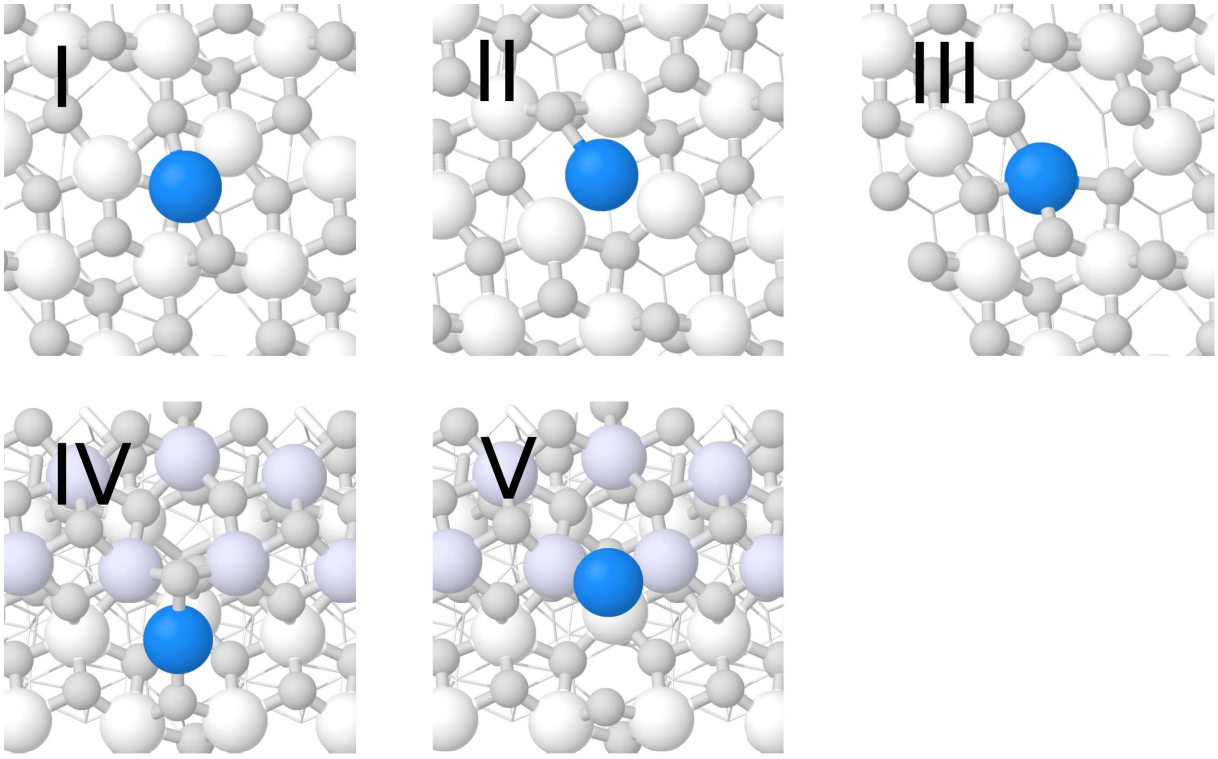

Figure S2: Rhodium single atoms deposited on the ideal (I), oxygen defected (II), and zirconium (III) defected zirconia terrace, and ideal (IV) and oxygen defected (V) zirconia edge. The Rh, O, and Zr atoms are coloured blue, grey, and white, respectively. For the edge models the Zr atoms on the upper step are lavender coloured for clarity.

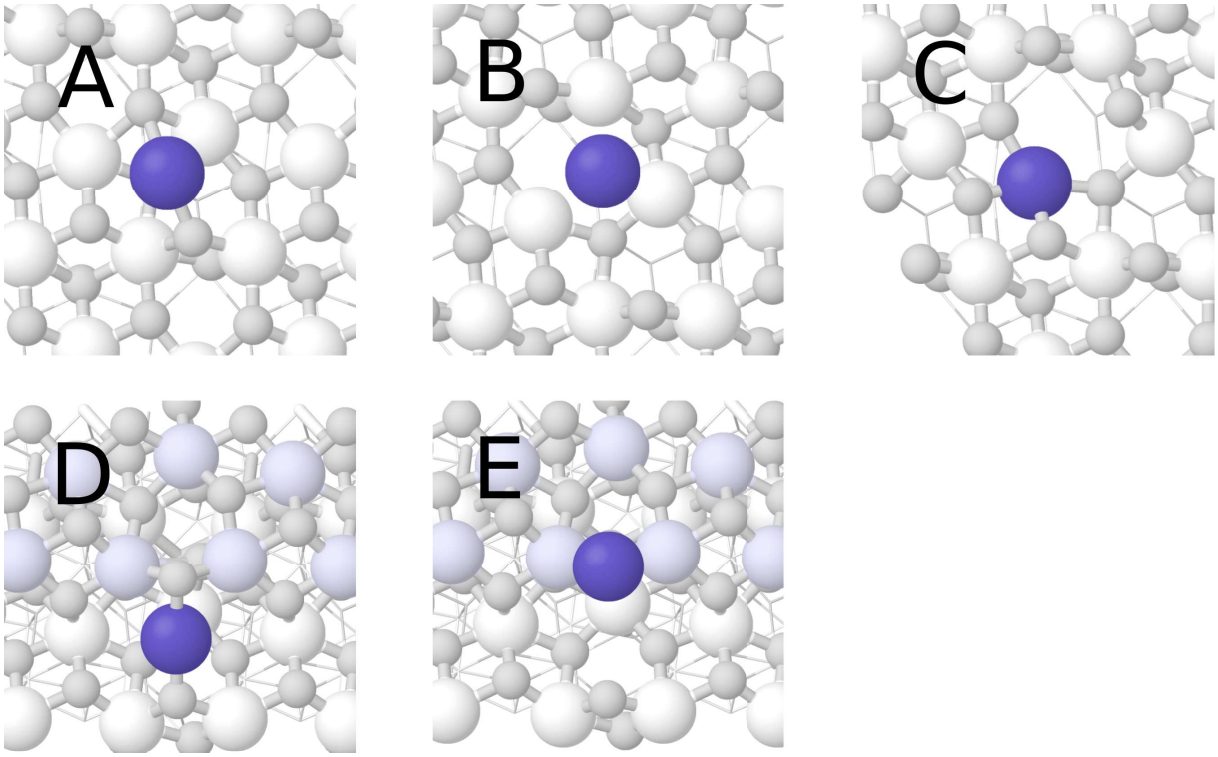

Figure S3: Structure geometries of the Platinum single atoms deposited on the ideal (A), oxygen defected (B), and zirconium (C) defected zirconia terrace, and ideal (D) and oxygen defected (E) zirconia edge. The Pt, O, and Zr atoms are coloured violet, grey, and white, respectively. For the edge models the Zr atoms on the upper step are lavender coloured for clarity.

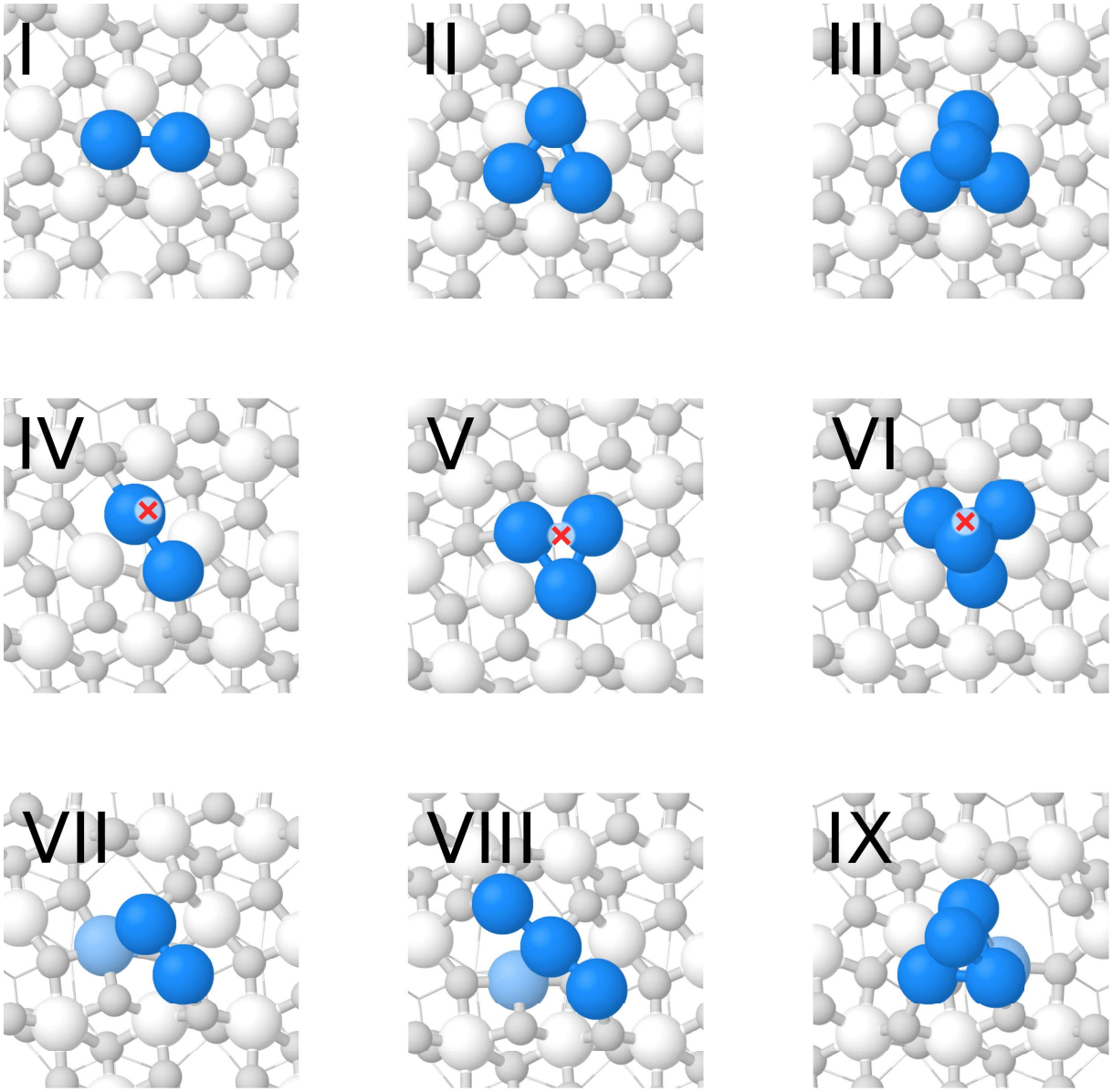

Figure S4: Structure geometries of the sub-nano Rh cluster models deposited on the ideal (I-III), oxygen defected (IV-VI), and zirconium defected (VII-IX) zirconia terrace. The Rh, O, and Zr atoms are coloured blue, grey, and white, respectively. For clarity, the approximate position of the oxygen vacancy in the underlying zirconia surface is marked with a red cross and the Rh atoms sitting in the zirconium vacancy site are coloured with a lighter blue than the other cluster atoms.

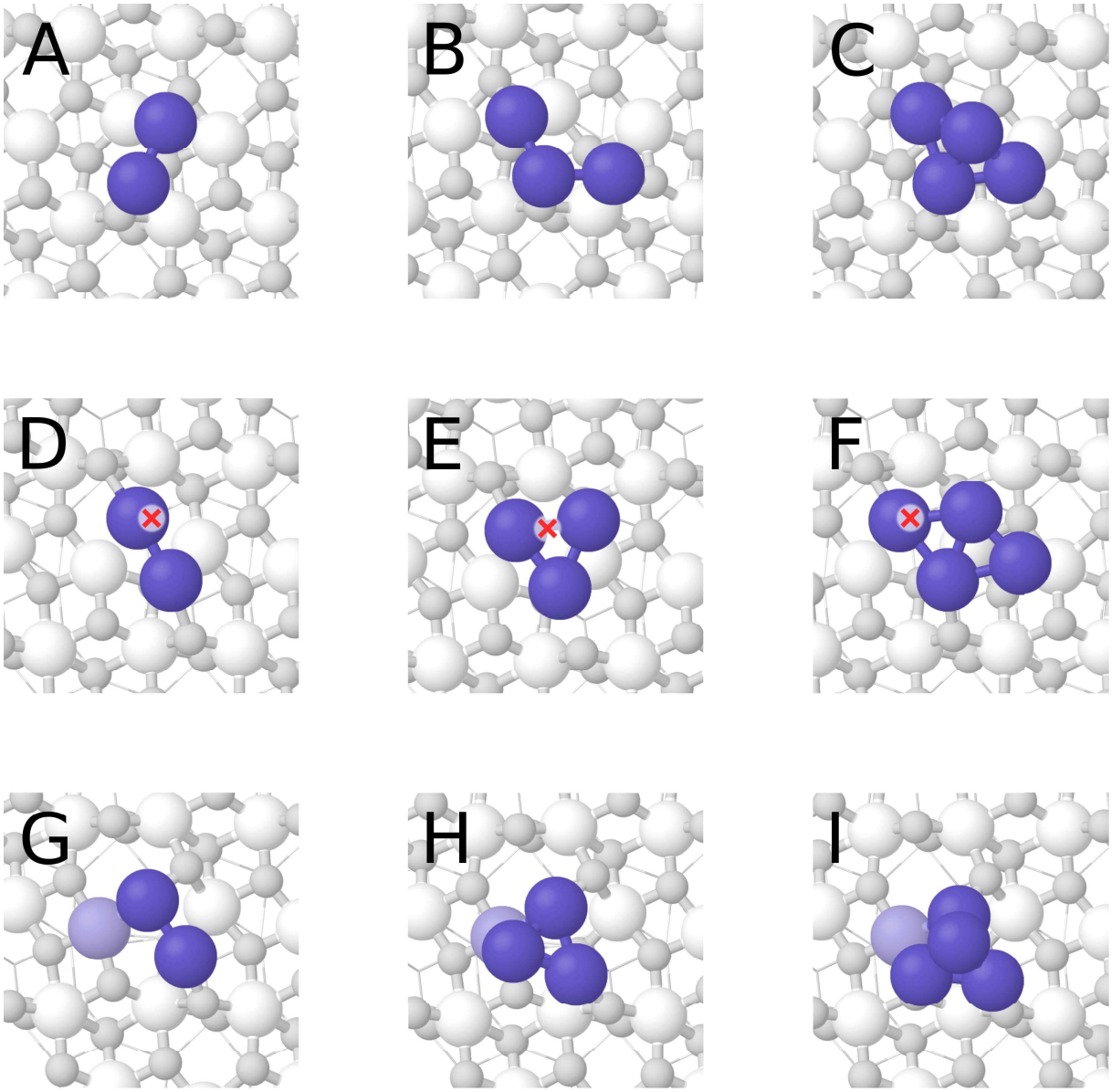

Figure S5: Structure geometries of the sub-nano Pt cluster models on the ideal (A-C), oxygen defected (D-F), and zirconium defected (G-I) zirconia terrace. The Pt, O, and Zr atoms are coloured violet, grey, and white, respectively. For clarity, the approximate position of the oxygen vacancy in the underlying zirconia surface is marked with a red cross and the Pt atoms sitting in the zirconium vacancy site are coloured with a lighter violet than the other cluster atoms.

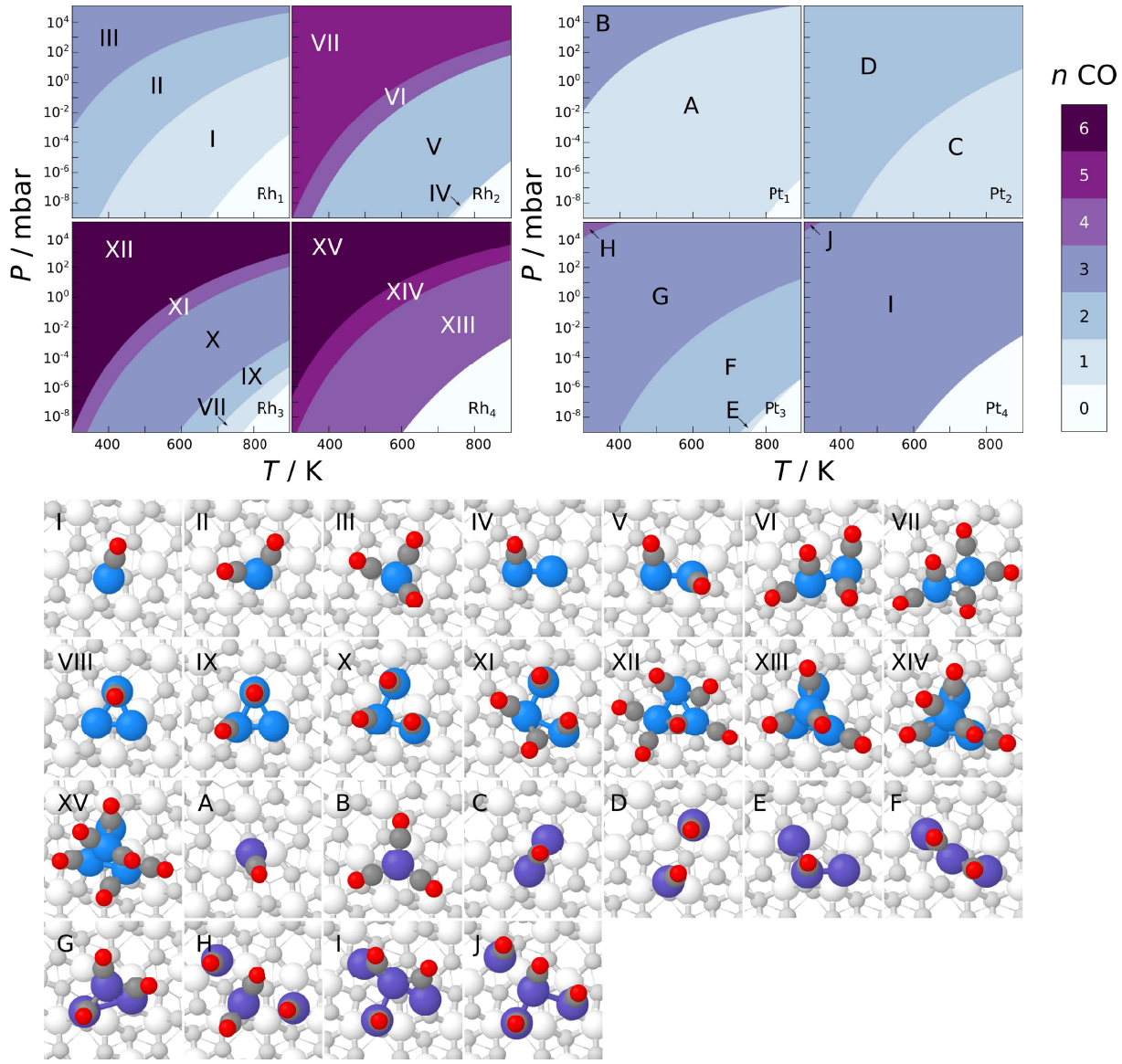

Figure S6: Phase diagrams showing the most stabilising amount of adsorbed CO on Rh (left) and Pt (right) 1-4 atom clusters on ideal zirconia as a function of CO pressure and temperature with corresponding structure images for Rh (I-XV) and Pt (A-J). The Rh, Pt, O, and Zr atoms are coloured blue, violet, grey, and white, respectively.

10 Density of states plots

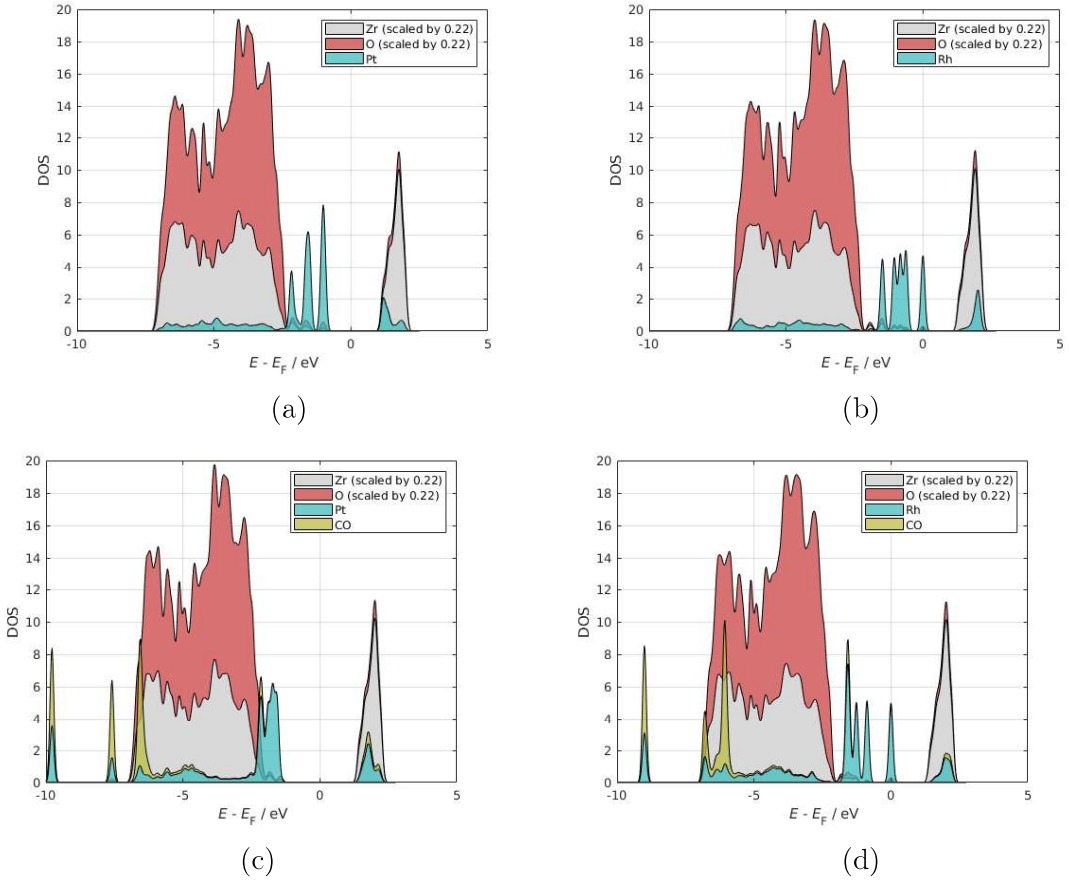

Figure S7: Density of states projected onto the orbitals of Zr, O, Pt, Rh, and CO, for the a) Pt_1/ZrO_2, b)Rh_1/ZrO_2, c)Pt_1-CO/ZrO_2, and d)Rh_1-CO/ZrO_2 systems.

References

(1) Ouyang, R.; Liu, J.-X.; Li, W.-X. Atomistic Theory of Ostwald Ripening and Disintegration of Supported Metal Particles under Reaction Conditions. *J. Am. Chem. Soc.* **2013**, *135*, 1760–1771, PMID: 23272702.

(2) Hammer, B.; Hansen, L. B.; Nørskov, J. K. Improved adsorption energetics within density-functional theory using revised Perdew-Burke-Ernzerhof functionals. *Phys. Rev. B* **1999**, *59*, 7413–7421.

(3) Klüpfel, S.; Klüpfel, P.; Jónsson, H. The effect of the Perdew-Zunger self-interaction correction to density functionals on the energetics of small molecules. *J. Chem. Phys.* **2012**, *137*, 124102.

(4) Komsa, H.-P.; Rantala, T. T.; Pasquarello, A. Finite-size supercell correction schemes for charged defect calculations. *Phys. Rev. B* **2012**, *86*, 045112.

(5) Reuter, K.; Scheffler, M. Surface core-level shifts at an oxygen-rich Ru surface: O/Ru(0001) vs. RuO2(110). *Surf. Sci.* **2001**, *490*, 20 – 28.

(6) Reuter, K.; Scheffler, M. First-Principles Atomistic Thermodynamics for Oxidation Catalysis: Surface Phase Diagrams and Catalytically Interesting Regions. *Phys. Rev. Lett.* **2003**, *90*, 046103.

(7) Reuter, K.; Scheffler, M. Composition, structure, and stability of $RuO_2(110)$ as a function of oxygen pressure. *Phys. Rev. B* **2001**, *65*, 035406.

(8) Larsen, A. H.; Mortensen, J. J.; Blomqvist, J.; Castelli, I. E.; Christensen, R.; Dułak, M.; Friis, J.; Groves, M. N.; Hammer, B.; Hargus, C.; Hermes, E. D.; Jennings, P. C.; Jensen, P. B.; Kermode, J.; Kitchin, J. R.; Kolsbjerg, E. L.; Kubal, J.; Kaasbjerg, K.; Lysgaard, S.; Maronsson, J. B.; Maxson, T.; Olsen, T.; Pastewka, L.; Peterson, A.; Rostgaard, C.; Schiøtz, J.; Schütt, O.; Strange, M.; Thygesen, K. S.; Vegge, T.; Vilhelmsen, L.; Walter, M.; Zeng, Z.; Jacobsen, K. W. The atomic simulation environment—a Python library for working with atoms. *J. Phys. Condens. Matter* **2017**, *29*, 273002.

(9) Bahn, S. R.; Jacobsen, K. W. An object-oriented scripting interface to a legacy electronic structure code. *Comput. Sci. Eng.* **2002**, *4*, 56–66.

(10) Kramida, A.; Yu. Ralchenko,; Reader, J.; and NIST ASD Team, NIST Atomic Spectra Database (ver. 5.5.6), [Online]. Available: `https://physics.nist.gov/asd` [2015, April 16]. National Institute of Standards and Technology, Gaithersburg, MD., 2018.

(11) Hill, T. L. Thermodynamics of Small Systems. *J. Chem. Phys.* **1962**, *36*, 3182–3197.

(12) Hill, T. L. A Different Approach to Nanothermodynamics. *Nano Lett.* **2001**, *1*, 273–275.

(13) Hill, T. L. *Thermodynamics of small systems. Parts I and II*; W.A. Benjamin, Inc, 1964.

(14) S.R. de Groot, P. M. *Non-equilibrium Thermodynamics*; Dover Publications, Inc., New York, 1984.

(15) Haase, R. *Thermodynamics of Irreversible Processes*; Addison-Wesley Publish Company, 1969.

(16) Naumovets, A.; Vedula, Y. Surface diffusion of adsorbates. *Surf. Sci. Rep.* **1985**, *4*, 365 – 434.

(17) Schnell, S. K.; Vlugt, T. J. H.; Simon, J.-M.; Bedeaux, D.; Kjelstrup, S. Thermodynamics of small systems embedded in a reservoir: a detailed analysis of finite size effects. *Mol. Phys.* **2012**, *110*, 1069–1079.

(18) Carrete, J.; Varela, L. M.; Gallego, L. J. Nonequilibrium nanothermodynamics. *Phys. Rev. E* **2008**, *77*, 022102.

(19) Reguera, D.; Rubí, J. M.; Vilar, J. M. G. The Mesoscopic Dynamics of Thermodynamic Systems. *J. Phys. Chem. B* **2005**, *109*, 21502–21515, PMID: 16853792.

(20) Wedekind, J.; Reguera, D. Kinetic Reconstruction of the Free-Energy Landscape. *J. of Phys. Chem. B* **2008**, *112*, 11060–11063, PMID: 18693697.

(21) Kemball, C. In *Entropy of Adsorption*; Frankenburg, W., Komarewsky, V., Rideal, E., Eds.; Adv. Catal.; Academic Press, 1950; Vol. 2; pp 233 – 250.